Journal of Power Sources 196 (2011) 6062–6069

Contents lists available at ScienceDirect

Journal of Power Sources

journal homepage: www.elsevier.com/locate/jpowsour

Reoxidation behavior of Ni–Fe bimetallic anode substrate in solid oxide fuel cells using a thin $LaGaO_3$ based film electrolyte

Young-Wan Ju[a,*], Shintaro Ida[a], Toru Inagaki[b], Tatsumi Ishihara[a]

[a] Department of Applied Chemistry, Faculty of Engineering, Kyushu University, Motooka 744, Nishi-Ku, Fukuoka 819-0395, Japan
[b] The Kansai Electric Power Co., Inc., 11-20 Nakoji 3-chome, Amagasaki, Hyogo 661-0974, Japan

ARTICLE INFO

Article history:
Received 25 December 2010
Received in revised form 16 March 2011
Accepted 29 March 2011
Available online 5 April 2011

Keywords:
$LaGaO_3$ electrolyte
Thin film
Metal support
Reoxidation

ABSTRACT

The reoxidation behavior of a Ni–Fe metal anode supported cell using a thin $LaGaO_3$ electrolyte film was investigated as a function of the reoxidation temperature. After oxidation and reduction treatments for 2 h, the voltage did not return to the initial voltage at higher temperatures (773–973 K); however, after reoxidation at 673 K, the cell exhibited almost the same OCV as the as-prepared cell. During reoxidation with air at the higher temperatures, the Ni–Fe metal substrate exhibited two different expansion behaviors by the different oxidation rates of Ni and Fe. On the other hand, the volumetric change of the oxidized substrate at 673 K was negligible. SEM-EDX results exhibited the reoxidation of Ni–Fe occurred only at the bottom part of the substrate and at the interface between the electrolyte and the substrate. In spite of temperatures as low as 673 K, the cell generated a power of 160 mW cm^{-2}, which hardly decreased after the redox cycle. The increasing anodic internal resistance accompanied with unreduced Fe.

© 2011 Elsevier B.V. All rights reserved.

1. Introduction

Solid oxide fuel cells (SOFCs) are regarded as future power generation systems having higher energy conversion efficiencies. For achieving high energy conversion efficiency, active electrode materials and low resistive electrolyte film are essentially requested for intermediate temperature SOFC (IT-SOFC). Other advantages of IT-SOFCs are their fuel flexibility and long service lives [1,2]. However, by decreasing the operation temperature, the power generation properties will be decreased by increasing the electrical resistances of the electrolytes because of large activation energy for oxide ion conductivity. Several investigations to reduce the internal resistances of electrolytes have been performed. The internal resistances of electrolytes depend on their ion conductivities and thicknesses; thus, the investigations focused on the discovery of new electrolyte materials [3–17] and the fabrication of thin electrolyte films [10–13,18–20].

Sr- and Mg-doped $LaGaO_3$ (LSGM) electrolytes are considered as alternatives to Y_2O_3-stabilized ZrO_2 electrolytes because these materials have high and stable oxygen ion conductivities over a wide range of oxygen partial pressures [3–13]. However, drawbacks of LSGM, such as the mismatch in its thermal expansion efficiency with conventional electrode materials and its reactivity with components in current SOFC systems, still hinder wider applications. In our previous work, we fabricated a thin electrolyte film of samarium-doped ceria ($Sm0_{.2}Ce_{0.8}O_{2-\delta}$, SDC)–LSGM ($La_{0.9}Sr_{0.1}Ga_{0.8}Mg_{0.2}O_{3-\delta}$) on a Ni–Fe metal substrate via the pulse laser deposition (PLD) method. The 10 wt% Fe-doped Ni substrate showed thermal expansion efficiency similar to LSGM and improved anodic activity [9]. In addition, after optimizing the sintering and reduction temperature, the cell displayed excellent power generation at intermediate temperatures [10–12]. Moreover, by inserting a thin interlayer of strontium-doped $SmCoO_3$ ($Sr_{0.5}Sm_{0.5}CoO_{3-\delta}$, SSC) between the LSGM electrolyte and the SSC cathode, its durability in the thermal cycle was improved [13].

However, for commercial applications of this anode-supported SOFC, further investigations, encompassing topics such as tolerance against reoxidation and long term stability, are necessary. Among them, the durability of the anode during reoxidation is significantly important for the reliability of this SOFC as a power generating system. Because the volumetric change of anode can occur by the reoxidation and causes permanent deactivation of the cell. In addition stopping procedure of the SOFC system becomes highly complex in case of emergency stop. In our previous study, we proposed the preparation of a porous Ni–Fe metal substrate via the reduction of a dense NiO–Fe_3O_4 disk by hydrogen with a volumetric change of less than 10%. However, this process suggested that the possibility of volumetric change during the reoxidation is limited for this substrate. Therefore, in this study, we investigated the tolerance of the Ni–Fe metal substrate during the redox cycle under actual operating conditions.

* Corresponding author. Tel.: +81 92 802 2868; fax: +81 92 802 2871.
E-mail address: ju_w@cstf.kyushu-u.ac.jp (Y.-W. Ju).

0378-7753/$ – see front matter © 2011 Elsevier B.V. All rights reserved.
doi:10.1016/j.jpowsour.2011.03.086

2. Experimental

A dense NiO–Fe_2O_3 composite oxide substrate was fabricated using an isostatic press by sintering at 1723 K for 5 h. According to our previously reported procedure, fine and uniform composite powder was prepared via the impregnation method and ball-milling in ethanol [10–14]. The diameter of fabricated anode substrate was 17 mm. On the dense substrate, a SDC–LSGM bi-layer film was deposited using the PLD method in commercial equipment (PLD-7, PASCAL). Before deposition, the substrate was heated to 1073 K, and the oxygen pressure was adjusted to 0.67 Pa by introducing commercial oxygen without purification. The laser power and frequency were controlled at 180 mJ $pulse^{-1}$ and 10 Hz, respectively. Optimized LSGM target composition ($La_{0.7282}Sr_{0.1}Ga_{0.6380}Mg_{0.4255}O_{3-\delta}$) and commercial SDC ($Sm_{0.2}Ce_{0.8}O_{2-\delta}$, Daiichi Kigenso Kagaku Kogyo Co. Ltd., Japan) were used to fabricate the LSGM electrolyte and the SDC interlayer, respectively. After post-annealing in air at 1073 K for 2 h, a thin, convex SSC layer was fabricated via the PLD method with an optimized SSC target composition ($Sm_{0.4}Sr_{0.6}Co_{1.6}O_{3-\delta}$) on the SDC–LSGM film. The diameter of deposited SSC layer was 5 mm. An SSC powder cathode was prepared by slurry coating on the SSC film and then fired at 1073 K for 30 min. In the meantime, a platinum wire was connected to the LSGM film near the cathode, as the reference electrode. To measure the power generation property of a single cell, humidified hydrogen (2.8 vol% H_2O) and commercial oxygen were fed into the cell as the fuel and the oxidant, respectively. It is noted that decrease in power density by changing oxygen to air for oxidant is not large for the used cell because the cathodic overpotential of $Sm_{0.5}Sr_{0.5}CoO_3$ is negligibly small. The flow rate of supplied oxidant and fuel was 100 ml min^{-1} (500 ml $(min\ cm^2)^{-1}$) and it is noted that fuel utilization is quite small in this experiment. Constant current was applied using a galvanostat (HA-301, Hokuto Denko), and the potential was measured using a digital multimeter (Advantest 6145). The internal resistances of the cell were analyzed via the current interruption method using a current pulse generator (Hokuto HC111) and a memory hicoder (Hioki 8835).

After sealing the cells at 800 K for 2 h, the cells were reduced at 973 K for 1 h. After achieving stable open circuit voltage (OCV), power generation property was measured at each temperature (673–973 K), and then the cell was reoxidized and reduced at temperature from 673 to 973 K for 2 h with commercial air and humidified hydrogen, respectively. Small current (20 mA cm^{-2}) was applied during the reoxidation by using a galvanostat (Hokuto Denko, HA-301). Before changing gas in anode side, gas line was purged with commercial nitrogen for 30 min. Volumetric change of Ni–Fe metal substrate was analyzed in oxidizing atmosphere by the thermomechanical analysis (TMA, Rigaku type 8310). Changes in porosity and volumetric shrinkage were investigated after the redox cycles. Reduction and reoxidation treatment was progressed in tubular furnace for 2 h with commercial hydrogen and oxygen, respectively. Porosity and density of substrates were measured by the Archimedes method with an immersion of deionized water [21]. Volumetric changes were measured by measurement of dimension of sample with micrometer.

In this study, it was investigated that reoxidation process dominates redox durability of the Ni–Fe metal supported SOFC. Before redox cycling, the power generation property at 973 K was confirmed. For electrochemical reoxidation, commercial nitrogen instead of humidified hydrogen was supplied to the anode. In the meantime, a small current (20 mA cm^{-2}) was supplied by using a galvanostat. After 1 h, nitrogen gas was again switched with humidified hydrogen and the current was reduced to zero. The chemical reoxidation of the substrate was performed with commercial air for 1 h at 973 K. Before switching the supplied gas, both gas-lines were purged with nitrogen gas. For the study of chemical oxidation effects, air in cathode site is switched to He when the fuel is changed to air from H_2. This is because the electrochemical reoxidation is suppressed by replacing oxygen with He. The reverse flow of oxygen ion is expected, however, this did not make serious problems because the experimental period is not long.

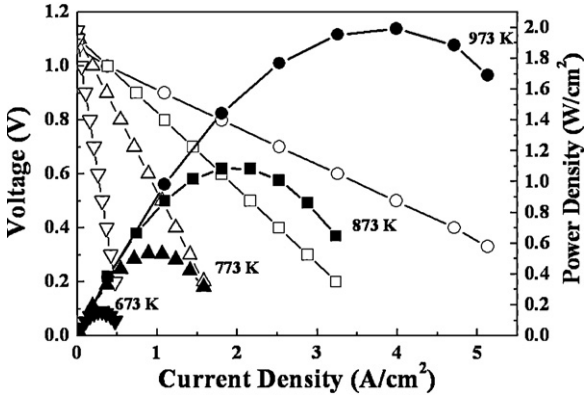

Fig. 1. Power generation properties of cell using LSGM–SDC bi-layer electrolyte film with a convex SSC interlayer as the electrolyte.

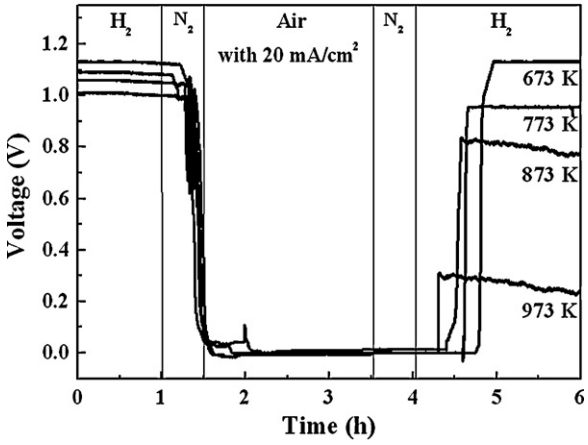

Fig. 2. Changes in the voltage during redox cycles with 20 mA cm^{-2} at 973 K, 873 K, 773 K, and 673 K.

3. Results and discussion

Fig. 1 shows the power generation properties of the LSGM–SDC bi-layer based single cell with SSC interlayer at intermediate temperatures. In the metal support cell design, a three-phase boundary (TPB) is formed only at the interface between the deposited electrolyte film and the metallic anode substrate. However, in spite of the narrow anodic TPB, the cell generated considerable electric power at each temperature. Even at operating temperatures as low as 673 K, the cell demonstrated a maximum power density of 0.16 W cm^{-2}. This power density was due to the high oxygen ion conductivity in the thin LSGM electrolyte film and the well developed micropores of the metallic anode substrate. In addition, the cell exhibited almost theoretical open circuit voltage (OCV) at all temperatures, implying that the deposited film possessed enough mechanical strength to overcome the physical stress caused by the reduction of the NiO–Fe_2O_3 substrate and the changes in the temperature. Therefore, an excellent tolerance against the redox cycle was expected. However, after reoxidation with air for 2 h, the voltage was not recover to the initial values despite supplying humidified hydrogen for 2 h at all temperatures except at 673 K as shown in Fig. 2. In particular, in the case of cells reoxidized at

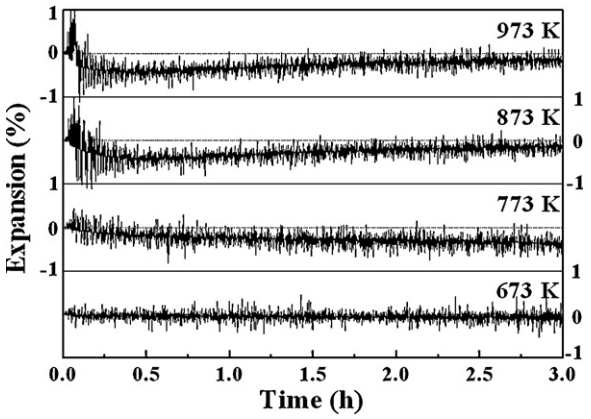

Fig. 3. Volumetric changes of the anode substrate during redox cycles over 3 h at 973 K, 873 K, 773 K, and 673 K.

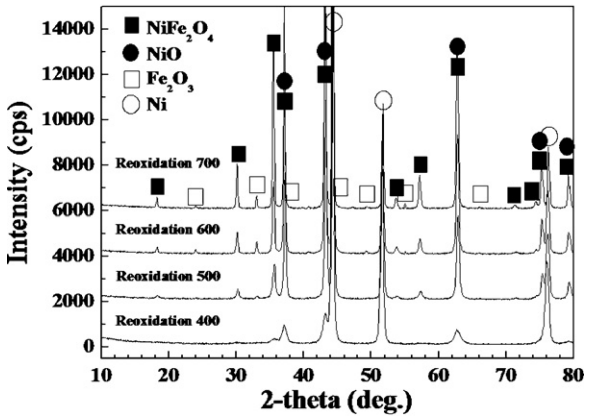

Fig. 4. XRD patterns of Ni–Fe bimetallic substrate after reoxidation for 3 h with air at different temperatures.

higher temperatures such as 973 K and 873 K, voltage decreased continuously after reaching stable voltage. In addition, the reoxidized cell at 773 K shows stable voltage, however, after secondary redox treatment, observed voltage decreased continuously with increasing fuel leakages. On the other hand, in the case of the cell reoxidized at 673 K, voltage was still stable and fuel-leakage was hardly observed after secondary redox treatment.

In order to confirm the reason of poor tolerance against the reoxidation, the effect of oxidation temperature on the Ni–Fe metal substrate was investigated. Fig. 3 shows a volumetric change of Ni–Fe substrates during the reoxidation treatment for 3 h at different temperatures. During re-oxidizing at 673 K, volumetric change of substrate was uncertain. On the other hand, other reoxidation temperature showed rapid expansion within an initial 10 min. After then, the substrate once shrank and then, expanded again gradually. These two expansions behaviors may be related with difference in oxidation rates of iron and nickel. Because iron is oxidized easily in oxidizing atmosphere in comparison with nickel, it can be expected iron in Ni–Fe alloy was oxidized and the oxidation of iron accompany with the expansion in volume. In addition, at the same time, the nickel decomposed from alloy was sintered and volumetric shrinkage was occurred. And then, nickel also oxidized gradually. Furthermore, according to these results, it can be suspected that high reoxidation temperature occur intense volume change accompanied with cracking of the deposited film.

XRD pattern of the reoxidized substrates was measured for understanding a complex volume change performance. Fig. 4 shows XRD patterns of reoxidized Ni–Fe substrates at different temperature. Despite of the reoxidation for 3 h in air, all substrates still showed strong diffraction peaks from Ni, while diffraction angle was shifted from pure Ni, suggesting alloy formation. Depending on oxidation temperature, the reoxidation level was changed, however, all samples shows specific peak of oxides such as $NiFe_2O_4$, NiO, and Fe_2O_3. However, as reported in our previous work, before reduction with hydrogen, the XRD pattern of the composite oxide substrate showed NiO and $NiFe_2O_3$ peaks [11,12]. In addition, after reduction, the XRD pattern showed only shifted Ni diffraction peaks, implying that all composite oxides were reduced completely to metal and that the added Fe seemed to form alloys with Ni. However, typical Fe_2O_3 peaks can be observed in the XRD pattern of the reoxidized substrate. Therefore, it can be said that the alloy was possibly decomposed because of the different oxidation rates of Ni and Fe during the reoxidation.

In this work, changes in the porosity of the substrate due to the redox cycles were also investigated with Archimedes method. Table 1 summarizes the volume, density, and porosity of the substrate. Before reduction, all sintered substrates were considerably dense with relative densities were approximately 98%. However, after reduction at 973 K for 2 h, the substrate changed into a porous form, and the porosity was then approximately 33%. Considering the hydrogen permeation rate, this porosity was sufficient for a porous substrate. However, after reoxidation at temperatures higher than 773 K, the porous substrates returned to their dense morphologies. On the other hand, the substrate reoxidized at 673 K

Table 1
Change of substrate in volume and density by redox cycle.

	Sample	Weight (g)	Volume (cm^3)	Density ($g\,cm^{-3}$)	Apparent density ($g\,cm^{-3}$)	Relate density (%)	Porosity (%)
NiFe-400	Initial	1.99	0.36	5.53	5.61	98.53	1.47
	Reduction	1.56	0.29	5.38	8.05	66.82	33.18
	Re-oxidation	1.57	0.29	5.41	6.18	87.6	12.4
	Reduction	1.56	0.29	5.38	8.04	66.91	33.09
NiFe-500	Initial	1.99	0.36	5.53	5.62	98.36	1.64
	Reduction	1.57	0.28	5.61	8.37	66.99	33.01
	Re-oxidation	1.58	0.27	5.85	6.02	97.21	2.79
	Reduction	1.58	0.27	5.83	8.48	68.79	31.21
NiFe-600	Initial	2.01	0.35	5.74	5.85	98.17	1.83
	Reduction	1.59	0.29	5.5	8.25	66.69	33.31
	Re-oxidation	1.65	0.27	6.2	6.33	97.99	2.01
	Reduction	1.61	0.26	6.17	8.55	72.15	27.85
NLFe-700	Initial	2.02	0.35	5.77	5.86	98.49	1.51
	Reduction	1.59	0.28	5.68	8.51	66.73	33.27
	Re-oxidation	1.68	0.27	6.22	6.34	98.14	1.86
	Reduction	1.63	0.25	6.42	8.03	79.92	20.08

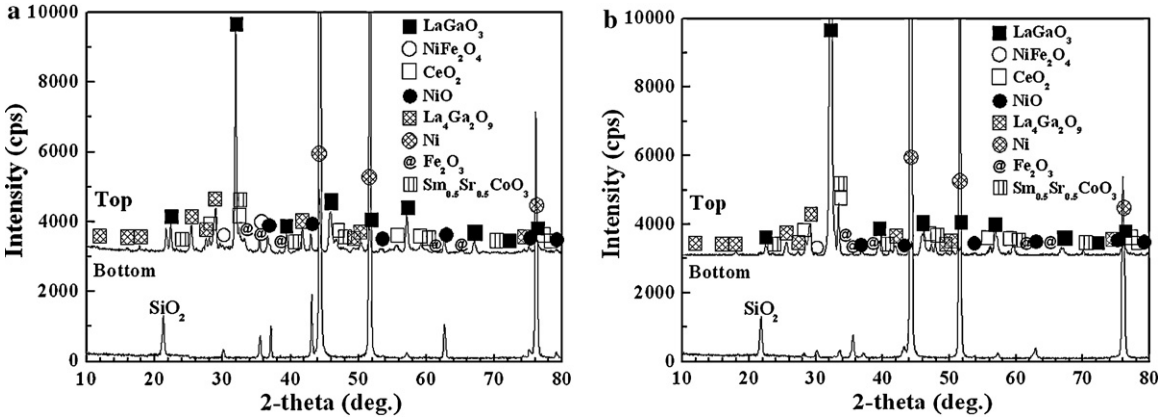

Fig. 5. (a) Surface and (b) cross-section image of the metal supported cells before reoxidation. (c) Surface morphology of reoxidized cell at 973 K, (d) cross-section of reoxidized cell at 773 K, and (e) surface morphology and (f) cross-section of reoxidized cell at 667 K.

was still slightly porous. In addition, after reduction at each temperature for 2 h, the oxidized substrates at 673 and 773 K exhibited almost the same porosities and volumes. However, in the case of substrates reoxidized at higher temperatures, despite the reduction at high temperature, the porosity was not recovered. Moreover, during the redox treatment, the substrate shrunk, and the weight increased. In accordance with these results, large difference in the oxidation rate was observed between Ni and Fe, therefore, nickel was separated from alloy phase and aggregated during reoxidation and some part of substrate still keep oxide state after reduction.

The effect of reoxidation on morphology in Ni–Fe supported cells was investigated by SEM observation. Fig. 5(a) and (b) shows surface and cross-section image of the Ni–Fe metal supported cell after the cell operation, respectively. The electrolyte exhibits dense surface morphology and is well-attached on the metal substrate. However, after reoxidation at 973 and 873 K, deposited film was partially delaminated and cracked as shown in Fig. 5(c). In this SEM image, it can be observed that Ni–Fe substrate has well-developed at grain boundary, which is related with shrinkage. Therefore, the poor tolerance against reoxidation at high temperature can be explained by the formation of crack and delamination of the deposited film occurring by the shrinkage of substrate during redox. On the other hand, the cell reoxidized at 773 and 673 K showed mostly dense surface morphology. However, reoxidized cell at 773 K showed a little crack and micro-gaps between deposited film and substrate as shown in Fig. 5(d). Fig. 5(e) and (f) shows the SEM image of surface and cross-section of reoxidized cell at 673 K. The deposited film is still dense and attached well on the substrate despite of secondary redox cycles. It certifies that the volumetric change of Ni–Fe substrate reoxidized at 673 K was negligibly small. However, in the cross-section image, some parts of substrate still show dense morphology. The dense part in the

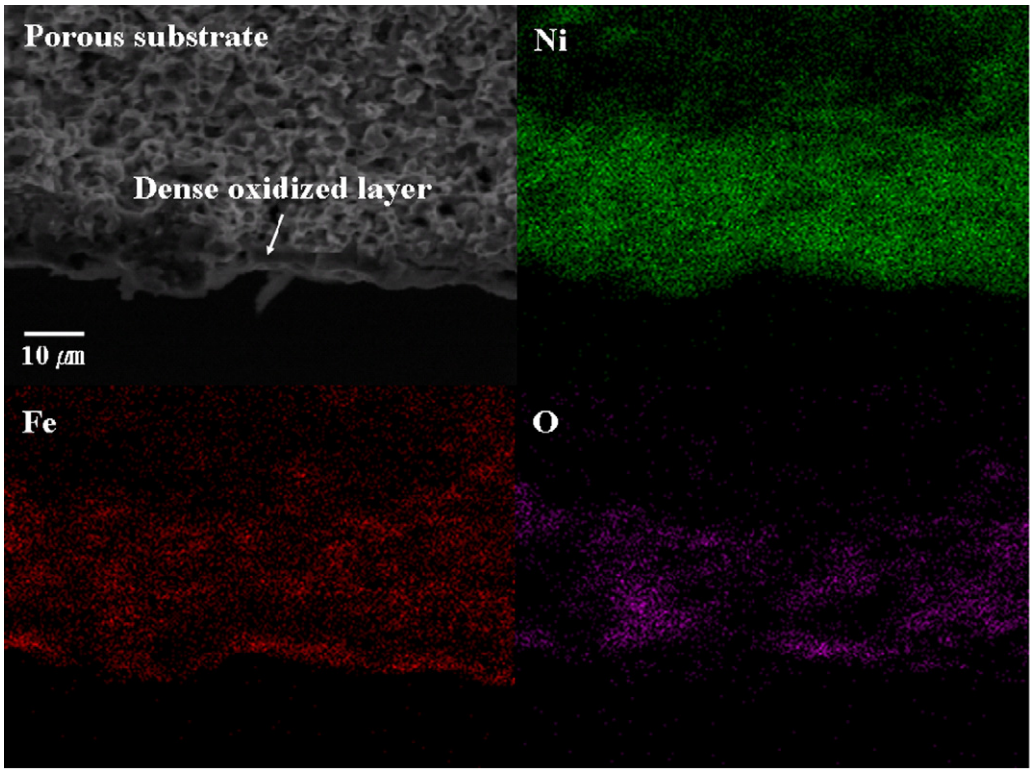

Fig. 6. EDX images of the bottom of the Ni–Fe metal substrate after redox cycle at 673 K.

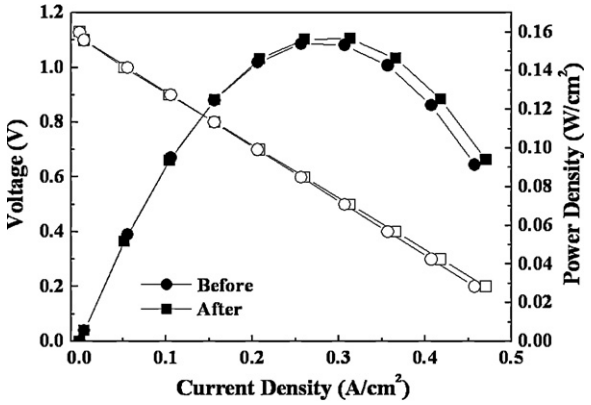

Fig. 7. Power generation property of the LSGM–SDC bi-layer electrolyte based cell before and after the redox cycle at 673 K.

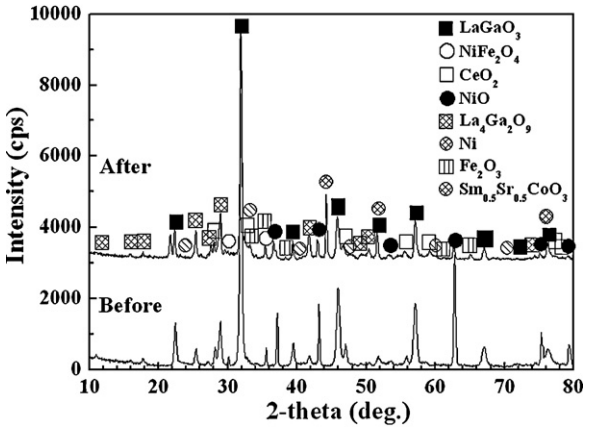

Fig. 9. XRD patterns of single cell before and after the redox cycle at 673 K.

substrate was observed only at the surface of substrate and the interface between electrolyte and substrate. Fig. 6 shows results of EDX analysis of the reoxidized substrate at 673 K. The results indicate that the dense part consists of oxides of Ni and Fe. After the reoxidation, the cell was reduced for an insufficient period of 2 h. However, the oxide part could not be attributed to the insufficient reduction period because the middle part of the substrate possessed a porous morphology. Sarantaridis et al. and Hatae et al. reported that the Ni near the electrolyte can be oxidized by oxide ions permeating through a thin electrolyte, i.e., by the electrochemical leakage of oxygen [22–25]. Therefore, the insufficient reduction state of the Ni–Fe at the interface between the electrolyte film and the metal substrate could be caused by such electrochemically leaked oxygen. Thus, further investigation is necessary to clarify such details.

On the other hand, in spite of oxide phase existing at interface, changes in OCV and gas-leakage were not observed after secondary redox cycles. However, power generation property was decreased slightly as shown in Fig. 7. In order to confirm the reason of decreased power density, internal resistance was measured in details with current interruption method, and obviously, increase in anodic internal resistance is a main reason (Fig. 8). Based on increasing anodic internal resistance, it may suspect the decreased activity accompanied with the decomposition of alloy and morphology changed by insufficient reduction. Fig. 9 shows XRD patterns of the cell before and after redox treatment at 673 K. It shows no significant change in crystal phase excepting for reduction of composite oxide substrate and appearance of Fe_2O_3. It also indicates that some part of interface between electrolyte and oxide was not reduced as mentioned above.

As before mentioned, two kind reoxidation process could be progressed during the redox cycling. One is electrochemical reoxidation caused by oxygen ion permeated through electrolyte. And other is chemical reoxidation occurred by oxygen in air gas. Therefore, in this study, it also was investigated which reoxidation process dominates redox durability of the Ni–Fe metal supported SOFC. Fig. 10 shows the voltage change during electrochemical reoxidation and reduction at 973 K. Before redox cycling, the cell exhibited the power generation property similar to that of previous results as shown in Fig. 1. After nitrogen was supplied and a small current was applied, the voltage reached to zero within 10 min. In addition, despite the short reoxidation time and the lack of an oxidant (such as air) at the anode, after reoxidation, the voltage was not recovered to its original value after exposure to hydrogen. In addition, fuel-leakage was increased significantly. This behavior is similar to that of the reoxidized cell at 973 K (Fig. 2). Fig. 11 shows the SEM images of the electrochemical reoxidized cell. In spite of the high reoxidation temperature and the poor reoxidation tolerance, a portion of the deposited film was still attached to the substrate without delaminating deposited film. However, the surface morphology showed slight cracking, and the cross-sectional image showed a considerable micro-gap at the interface between the deposited film and the substrate. In addition, the cross-sectional image shows dense oxide part at the interface between the substrate and the electrolyte. This dense oxide part existed at only

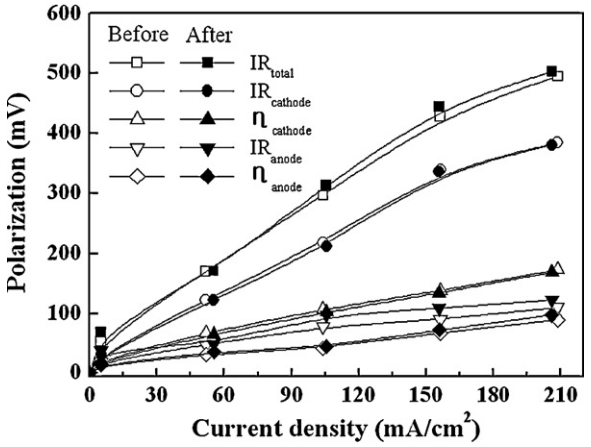

Fig. 8. Internal resistance of the Ni–Fe metal-supported LSGM–SDC cell at 673 K before and after the redox cycle.

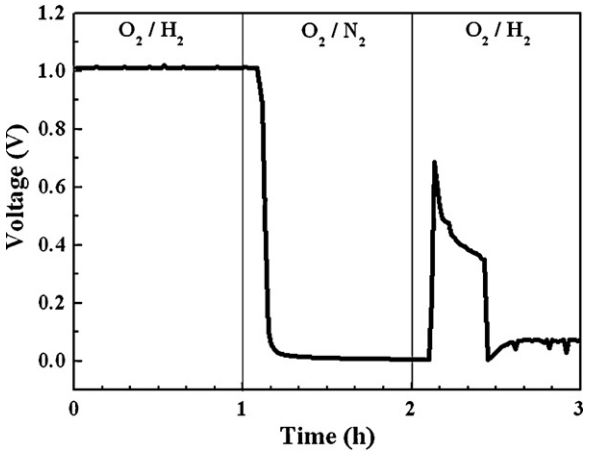

Fig. 10. Changes in voltage of the electrochemical redox treated cell with 20 mA cm^{-2} at 973 K.

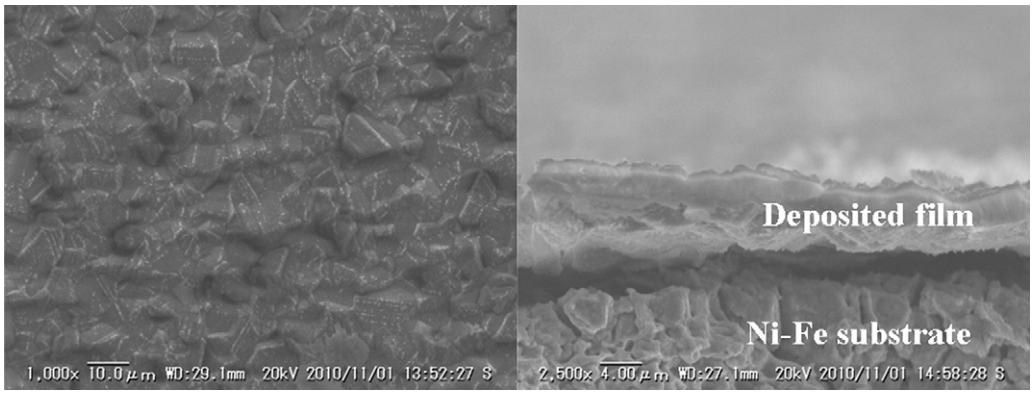

Fig. 11. SEM images of electrochemically reoxidized cell at 973 K.

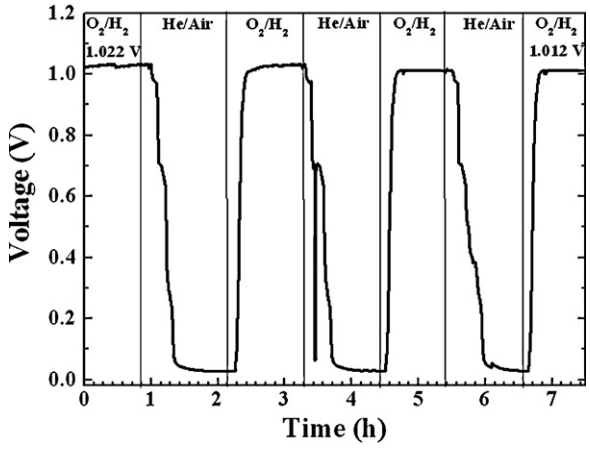

Fig. 12. Changes in voltage of chemically redox treated cell at 973 K.

the interface. It indicates the interface was reoxidized by the oxygen ion electrochemically pumped though electrolyte. Therefore, it can be suspected the reoxidation accompany with the volumetric change of the substrate, which cause the formation of micro-gap at interface during the redox cycle. This is because the reoxidation is occurred at the interface between electrolyte and anode substrate.

On the other hand, the chemical reoxidized cell exhibited small degradation in the voltage and small increase in the gas leakage after the redox cycles. However, even after the third redox cycle at the high temperature, the voltage of the cell recovered to similar voltage as shown in Fig. 12. Even though the short reoxidation period was considered, this fact indicates that the effect of chemical reoxidation on the redox tolerance was negligible compared to that of electrochemical reoxidation. Therefore, the tolerance of the Ni–Fe metal-supported cell during the redox cycle was dominated by the electrochemical reoxidation of the interface between the electrolyte and the substrate. Fig. 13 shows the SEM images of the cell chemically reoxidized at 973 K. Even after third redox cycles, the deposited film still exhibited a dense surface without any cracks. The cross-sectional image depicts a film well attached on a porous substrate, and there were no dense oxide parts at the interface, implying that electrochemical reoxidation did not occur during the redox cycles. Therefore, it can be suspected that fuel-leakages originated from the breaking of the glass ring used as the sealing agent.

Fig. 14(a) shows the power generation properties of the cell chemically reoxidized with air at 973 K. Before the redox cycle, the cell exhibited a similar power generation property to the previous results at 973 K (Fig. 1). However, after the redox cycle, the power generating performance of the cell at 973 K decreased slightly. In addition, the cell demonstrated a lower power density at the low temperature than that of the previous results. This might be attributed to the increasing fuel leakage during the redox cycle. However, the cell still showed a high power generation property. Moreover, the fuel leakage did not increase any more during changing the temperature because of the gas-tight structure, as shown in the SEM image (Fig. 13). Fig. 14(b) shows the internal resistance of the cell at 973 K before and after the chemical redox cycling. After the redox cycle, the cathodic IR loss and overpotential slightly changed. On the other hand, the anodic internal resistance increased significantly. Particularly, the anodic IR loss increased considerably after the redox cycles. This behavior was similar to that of the cell reoxidized at 673 K as shown in Fig. 8. Therefore, it can be said that the increasing anodic IR loss possibly originated from the partial reoxidation of the Ni–Fe substrate. Fig. 15 shows

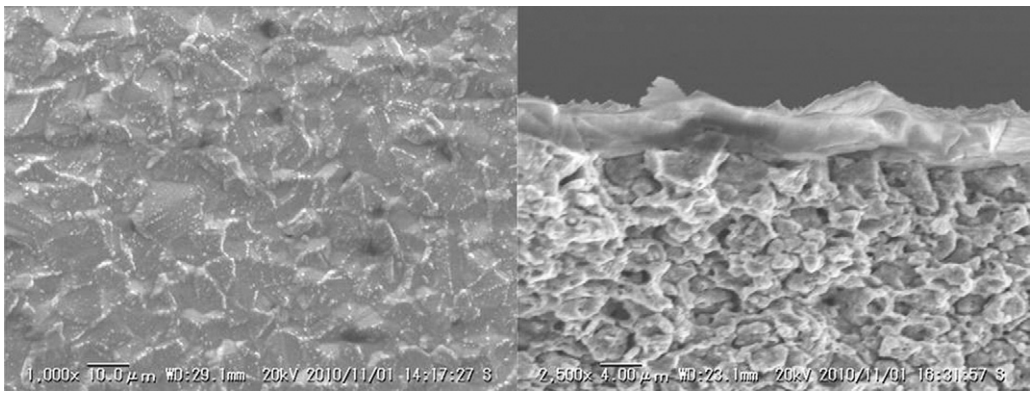

Fig. 13. SEM images of chemically reoxidized cell at 973 K.

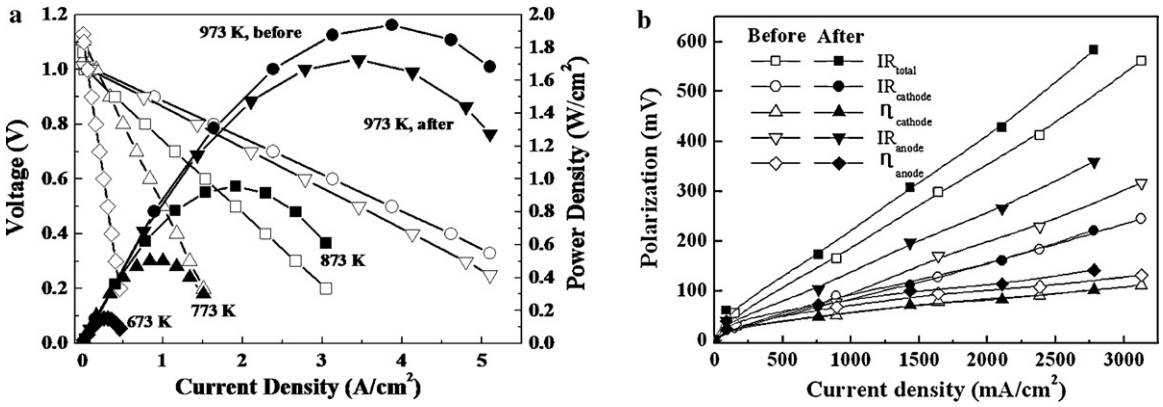

Fig. 14. (a) Power generation property and (b) changes in internal resistance at 973 K chemically reoxidized cell.

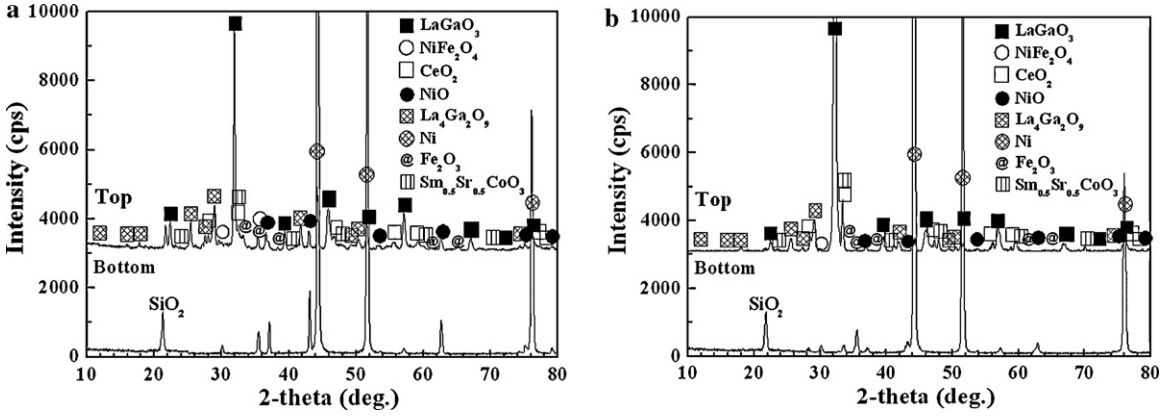

Fig. 15. XRD patterns of chemically reoxidized cell at 973 K.

the XRD patterns of the chemically reoxidized cell and those of the electrochemically reoxidized cell. For the case of the electrochemically reoxidized cell (Fig. 15(a)), the diffraction peaks from the top side consisted of some oxide peaks with typical Fe_2O_3 peaks; however, those from the bottom side of the substrate were strong-Ni and weak-Ni based oxides peaks. On the other hand, the chemically reoxidized cell (Fig. 15(b)) showed no Ni based oxide and Fe based oxide peaks from the top side, but the bottom of substrate showed not only Ni and Ni based oxide peaks but also Fe_2O_3 peaks. These results prove that individual reoxidation separated successively simply by controlling the supplied gas. In addition, they also prove that reoxidation of the Ni–Fe substrate occurred only at the bottom side via chemical reoxidation. Therefore, it can be said that the volumetric change possibly occurred only at the bottom of the substrate, and the Ni–Fe metal supported cell exhibits excellent tolerance against chemical reoxidation.

4. Conclusions

In this study, the redox behavior of a Ni–Fe metal anode substrate was investigated at different temperatures. After the reduction, a 10 wt% Fe_2O_3-doped NiO composite oxide substrate changed to a metal substrate consisting of Ni–Fe alloy. However, even after reoxidation for 3 h, the substrate still contained a large amount of alloy. During reoxidation, the high reoxidation temperature caused a two-step volumetric expansion because of the different reoxidation rates of Ni and Fe. These volumetric changes accompanied with the delaminating deposited film and also decreased the power density. On the other hand, reoxidation at 673 K resulted in negligible volumetric change in the Ni–Fe substrate and exhibited excellent durability during the redox cycle. However, after the redox treatment, the LSGM–SDC bi-layer based cell showed a small degradation in the power generation property. This degradation was caused by the changes in the anodic activity and the morphology of the anode substrate. However, the cell still generated a high electric power despite the low operating temperature. In addition, the effects of individual reoxidations, which were both chemical and electrochemical, were investigated. Chemical reoxidation exhibited slight degradation in the power generation property despite the high redox temperature. On the other hand, electrochemical reoxidation with oxygen ions exhibited poor tolerance during the redox cycle. Therefore, it can be said the chemical reoxidation dominated the redox tolerance in the Ni–Fe metal supported cell.

References

[1] S.C. Singhal, Solid State Ionics 152–153 (2002) 405.
[2] N.Q. Minh, Solid State Ionics 174 (1–4) (2004) 271.
[3] T. Ishihara, H. Matsuda, Y. Takita, J. Am. Chem. Soc. 116 (1994) 3801.
[4] T. Ishihara, H. Minami, H. Matsuda, H. Nishiguchi, Y. Takita, Chem. Commun. 8 (1996) 929.
[5] T. Ishihara, M. Honda, T. Shibayama, H. Minami, H. Nishiguchi, Y. Takita, J. Electrochem. Soc. 145 (1998) 3177.
[6] J.W. Yan, Z.G. Lu, Y. Jiang, Y.L. Dong, Y.C. Yu, W.Z. Li, J. Electrochem. Soc. 149 (2002) A1132.
[7] S. Wang, T. Chen, S. Chen, J. Electrochem. Soc. 151 (2004) A1461.
[8] J.W. Yan, H. Matsumoto, M. Enoki, T. Ishihara, Electrochem. Solid-State Lett. 8 (2005) A389.
[9] T. Ishihara, J.W. Yan, M. Shinagawa, H. Matsumoto, Electrochim. Acta 52 (2006) 1645.
[10] Y.W. Ju, H. Matsumoto, T. Ishihara, T. Inagaki, H. Eto, J. Korean Ceram. Soc. 45 (2008) 796.
[11] Y.W. Ju, H. Eto, T. Inagaki, T. Ishihara, ECS Trans. 25 (2009) 719.
[12] Y.W. Ju, H. Eto, T. Inagaki, S. Ida, T. Ishihara, J. Power Sources 195 (2010) 6294.

[13] Y.W. Ju, H. Eto, T. Inagaki, S. Ida, T. Ishihara, Electrochem. Solid-State Lett. 13 (2010) B139.
[14] M. Mogensen, N.M. Sammes, G.A. Tompsett, Solid State Ionics 129 (2000) 63.
[15] J.B. Goodenough, Ann. Rev. Mater. Res. 33 (2003) 91.
[16] V.V. Kharton, F.M.B. Marques, A. Atkinson, Solid State Ionics 174 (2004) 135.
[17] J.W. Fergus, J. Power Sources 162 (2006) 30.
[18] C.C. Chen, M.M. Nasrallah, H.U. Anderson, Solid State Ionics 70–71 (1994) 101.
[19] S. de Souza, S.J. Visco, L.C. De Jonghe, Solid State Ionics 98 (1997) 57.
[20] C.J. Li, C.X. Li, Y.Z. Xing, M. Gao, G.J. Yang, Solid State Ionics 177 (2006) 2065.
[21] ASTM B962-08. Standard Test Methods for Density of Compacted or Sintered Powder Metallurgy (PM) Products Using Archimedes' Principle. Annual Book of ASTM Standards, vol. 02.05. West Conshohocken, PA: American Society for Testing and Materials.
[22] D. Sarantaridis, R.J. Chater, A. Atkinson, J. Electrochem. Soc. 155 (2008) B467.
[23] D. Sarantaridis, R.A. Rudkin, A. Atkinson, J. Power Sources 180 (2008) 704.
[24] T. Hatae, Y. Matsuzaki, Y. Yamazaki, Solid State Ionics 179 (2008) 274.
[25] T. Hatae, Y. Matsuzaki, S. Yamashita, Y. Yamazaki, Solid State Ionics 180 (2009) 1305.